be used to test the optical quality of another optical component, such as a prism, situated as shown in Figure 8-4b. Surface imperfections or internal variations in refractive index show up as a distortion of the fringe pattern. Lenses are tested for aberrations in the same way, once plane mirror $M1$ is replaced by a convex spherical surface that can reflect the refracted rays back along themselves, as suggested in the inset of Figure 8-4b.

Mach-Zehnder Interferometer

A more radical variation, sketched in Figure 8-5, is the Mach-Zehnder interferometer. The incident beam of roughly collimated light is divided into two beams at beam splitter BS. Each beam is again totally reflected by mirrors $M1$ and $M2$, and the beams are made coincident again by the semitransparent mirror $M3$. Path lengths of beams 1 and 2 around the rectangular system and through the glass of the beam splitters are identical. This interferometer has been used, for example, in aerodynamic research, where the geometry of air flow around an object in a wind tunnel is revealed through local variations of pressure and refractive index. A windowed test chamber, into which the model and a streamlined flow of air is introduced, is placed in path 1. An identical chamber is placed in path 2 to maintain equality of optical paths. The air-flow pattern is revealed by the fringe pattern. For such applications the interferometer must be constructed on a rather large scale. An advantage of the Mach-Zehnder over the Michelson interferometer is that, by appropriate small rotations of the mirrors, the fringes may be made to appear at the object being tested, so that both can be viewed or photographed together. In the Michelson interferometer, fringes appear localized on the mirror and so cannot be seen in sharp focus at the same time as a test object placed in one of its arms.

The Michelson, Twyman-Green, and Mach-Zehnder interferometers are all two-beam interference instruments that operate by division of amplitude. We turn now to an important case of a multiple-beam instrument, the Fabry-Perot interferometer.

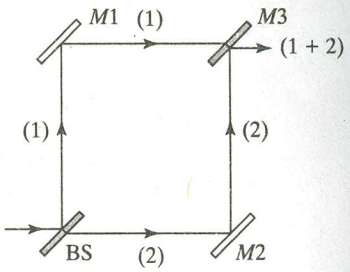

Figure 8-5 Mach-Zehnder interferometer.

8-4 THE FABRY-PEROT INTERFEROMETER

The Fabry-Perot interferometer makes use of an arrangement similar to the plane parallel plate, discussed in Section 7-9, to produce an interference pattern that results from the superposition of the multiple beams of the transmitted light. This instrument, probably the most adaptable of all interferometers, has been used, for example, in precision wavelength measurements, analysis of hyperfine spectral line structure, determination of refractive indices of gasses, and the calibration of the standard meter in terms of wavelengths. Although simple in structure, it is a high-resolution instrument that has proven to be a powerful tool in a wide variety of applications.

A possible arrangement is shown in Figure 8-6. Two thick glass or quartz plates are used to enclose a plane parallel "plate" of air between them, which forms the medium within which the beams are multiply reflected. The glass plates function as mirrors and the arrangement is often called

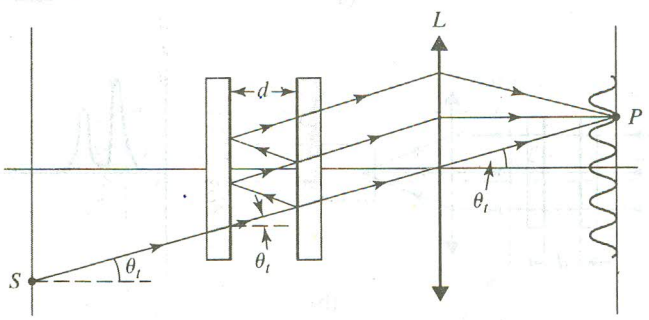

Figure 8-6 Fabry-Perot interferometer.

a *cavity*. The important surfaces of the glass plates are therefore the inner ones. Their surfaces are generally polished to a flatness of better than $\lambda/50$ and coated with a highly reflective layer of silver or aluminum. Silver films are most useful in the visible region of the spectrum, but their reflectivity drops off sharply around 400 nm, so that for applications below 400 nm, aluminum is usually used. Of course, the films must be thin enough to be partially transmitting. Optimum thicknesses for silver coatings are around 50 nm. The outer surfaces of the glass plate are purposely formed at a small angle relative to the inner faces (several minutes of arc are sufficient) to eliminate spurious fringe patterns that can arise from the glass itself acting as a parallel plate. The spacing, or thickness, d of the air layer, is an important performance parameter of the interferometer, as we shall see. When the spacing is fixed, the instrument is often referred to as an *etalon*.

Consider a narrow, monochromatic beam from an extended source point S making an angle (in air) of θ_t with respect to the optical axis of the system, as in Figure 8-6. The single beam produces multiple coherent beams in the interferometer, and the emerging set of parallel rays are brought together at a point P in the focal plane of the converging lens L. The nature of the superposition at P is determined by the path difference between successive parallel beams, $\Delta = 2n_f d \cos\theta_t$. Using $n_f = 1$ for air, the condition for brightness is

$$2d \cos\theta_t = m\lambda \tag{8-15}$$

Other beams from different points of the source but in the same plane and making the same angle θ_t with the axis satisfy the same path difference and also arrive at P. With d fixed, Eq. (8-15) is satisfied for certain angles θ_t, and the fringe system is the familiar concentric rings due to the focusing of fringes of equal inclination. When a collimating lens is used between source and interferometer, as shown in Figure 8-7a, every set of parallel beams entering the etalon must arise from the same source point. A one-to-one correspondence then exists between source and screen points. The screen may be the retina or a photographic plate. Figure 8-7b illustrates another arrangement, in which the source is small. Collimated light in this instance reaches the plates at a fixed angle θ_t ($\theta_t = 0$ is shown) and comes to a focus at a light detector. As the spacing d is varied, the detector records the interference pattern as a function of time in an *interferogram*. If, for example, the source light consists of two wavelength components, the output of the two systems is either a double set of circular fringes on a photographic plate or a plot of resultant irradiance

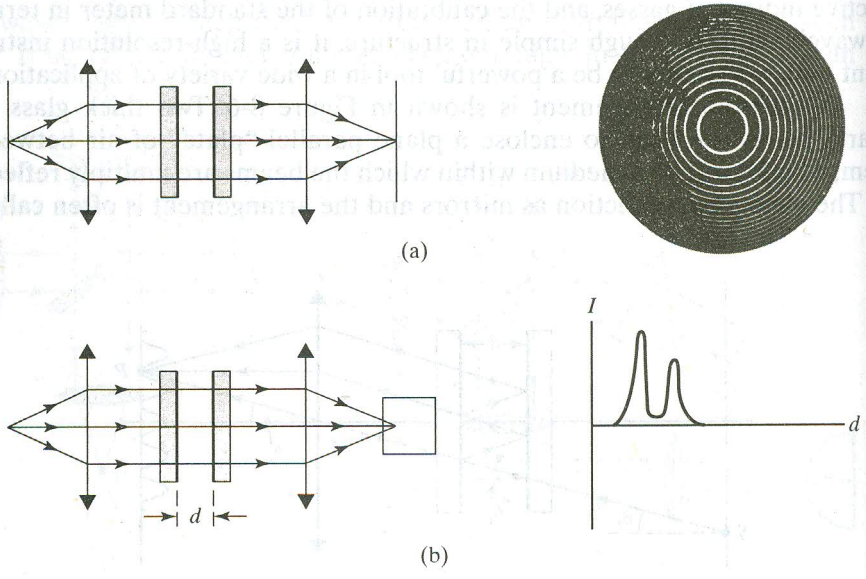

Figure 8-7 (a) Fabry-Perot interferometer, used with an extended source and a fixed plate spacing. A circular fringe pattern like the one shown may be photographed at the screen. (Photo from M. Cagnet, M. Francon, and J. C. Thrierr, *Atlas of Optical Phenomenon*, Plate 10, Berlin: Springer-Verlag, 1962.) (b) Fabry-Perot interferometer, used with a point source and a variable plate spacing. A detector at the focal point of the second lens records intensity as a function of plate spacing d. If a laser source is used, the lenses may not be needed.

I versus the plate spacing d, as suggested in Figure 8-7b. In many common applications the source is a laser, in which case the lenses shown in Figure 8-7b may not be needed. It is this last arrangement that we will discuss in the following sections.

8-5 FABRY-PEROT TRANSMISSION: THE AIRY FUNCTION

The irradiance transmitted through a Fabry-Perot interferometer can be calculated with the help of the analysis used to treat the parallel plate arrangement of Section 7-9. In this section we present an alternative method that can also be used to determine the loss rate of a laser cavity. Consider the arrangement of Figure 8-8. We will assume that the two mirrors that form the Fabry-Perot cavity are identical, are separated by a distance d, and have real (internal surface) electric-field reflection and transmission coefficients r and t. Further, we will assume that an electric field suffers no absorption upon encountering the cavity mirrors, so that

$$r^2 + t^2 = 1 \qquad \text{lossless mirrors} \tag{8-16}$$

A useful parameter associated with the Fabry-Perot interferometer is the cavity round-trip time τ. The cavity round-trip time is the time needed for light to circulate once around the cavity and so is given by

$$\tau = 2d/v = 2nd/c$$

Here, $v = c/n$ is the speed of light in the medium filling the space between the mirrors, n is the index of refraction of this medium, and c is the speed of light in vacuum.

We wish to express the electric field E_T transmitted through the Fabry-Perot interferometer in terms of the field E_I incident on the interferometer, the reflection coefficient r of the cavity mirrors, and the length d of the cavity. In the analysis that follows, we will make use of the notion of a *propagation factor* $P_F(\Delta z, \Delta t)$. As we define it, the propagation factor is the ratio of an electric field $E(z, t)$ associated with a traveling monochromatic plane wave at position $z = z_0 + \Delta z$ and time $t = t_0 + \Delta t$ to the same electric field at position $z = z_0$ and time $t = t_0$. That is,

$$E(z_0 + \Delta z, t_0 + \Delta t) = P_F(\Delta z, \Delta t)E(z_0, t_0)$$

For example, for a plane monochromatic wave traveling in the $+z$ direction encountering no changes in optical media,

$$P_F(\Delta z, \Delta t) = \frac{E(z_0 + \Delta z, t_0 + \Delta t)}{E(z_0, t_0)} = \frac{E_0 e^{i[\omega(t_0+\Delta t)-k(z_0+\Delta z)]}}{E_0 e^{i(\omega t_0 - k z_0)}} = e^{i(\omega \Delta t - k \Delta z)} \tag{8-17}$$

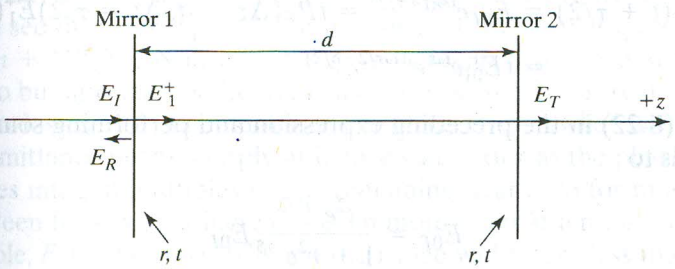

Figure 8-8 Schematic of a Fabry-Perot interferometer consisting of two mirrors with reflection and transmission coefficients r and t. The electric field incident on the interferometer from the left is E_I, the reflected field is E_R, the transmitted field is E_T, and E_1^+ is the right-going intracavity field at Mirror 1.

We choose not to include electric field changes caused by reflection from or transmission through mirrors in the definition of the propagation factor, but rather we will include these factors explicitly when we track changes to an electric field that encounters mirrors.

To determine the field transmitted through the Fabry-Perot cavity, it is convenient to first determine the amplitude of the intracavity right-going electric field shown as E_1^+ in Figure 8-8. Proceeding, we write the right-going (traveling in the $+z$ direction) electric field incident on the Fabry-Perot cavity from the left as

$$E_I = E_{0I}e^{i\omega t} \tag{8-18}$$

and the right-going electric field in the cavity, at the position of the first mirror as,

$$E_1^+ = E_{01}^+(t)e^{i\omega t} \tag{8-19}$$

Note that the amplitude of this field is, in general, time dependent to allow for the buildup or decay of the intracavity field as the incident field is turned on or off. At time $t + \tau$, the right-going intracavity field $E_1^+(t + \tau)$ can be formed as the sum of two parts. One part is the fraction of the incident field $tE_I(t + \tau)$ that is transmitted through Mirror 1 at this time. The other part is the fraction $r^2P_F(\Delta z = 2d, \Delta t = \tau)E_1^+(t)$ of the entire right-going intracavity field that existed at Mirror 1 one cavity round-trip time τ earlier. This latter part has propagated around the cavity a distance $2d$ in a time τ, reflecting once from each mirror and returning back to Mirror 1 at time $t + \tau$. That is,

$$E_1^+(t + \tau) = tE_I(t + \tau) + r^2P_F(\Delta z = 2d, \Delta t = \tau)E_1^+(t) \tag{8-20}$$

Using Eqs. (8-17) through (8-19) in Eq. (8-20) gives

$$E_{01}^+(t + \tau)e^{i\omega(t+\tau)} = tE_{0I}e^{i\omega(t+\tau)} + r^2E_{01}^+(t)e^{i\omega t}e^{i(\omega\tau - 2kd)}. \tag{8-21}$$

Some time after the incident field is first directed onto the cavity, the intracavity electric field will settle down to a constant steady-state value. Once such a steady state has been reached, $E_{01}^+(t + \tau) = E_{01}^+(t) \equiv E_{01}^+$. In steady state, Eq. (8-21) can be solved for the intracavity right-going field amplitude E_{01}^+,

$$E_{01}^+ = \frac{t}{1 - r^2e^{-i\delta}}E_{0I} \tag{8-22}$$

Here,

$$\delta = 2kd$$

is the round-trip phase shift.

The transmitted field E_T can be found by propagating the right-going cavity field E_1^+ at Mirror 1 through the cavity and out of Mirror 2,

$$\begin{aligned} E_T(t + \tau/2) &= E_{0T}e^{i\omega(t+\tau/2)} = tP_F(\Delta z = d, \Delta t = \tau/2)E_1^+(t) \\ &= tE_{01}^+e^{i\omega t}e^{i(\omega\tau/2 - \delta/2)} \end{aligned}$$

Using Eq. (8-22) in the preceding expression and performing some simplification leads to

$$E_{0T} = \frac{t^2e^{-i\delta/2}}{1 - r^2e^{-i\delta}}E_{0I} \tag{8-23}$$

Irradiance is proportional to the square of the magnitude of the field amplitude, $I_T \propto E_{0T}E_{0T}^*$, so the transmittance T of the Fabry-Perot cavity is

$$T \equiv \frac{I_T}{I_I} = \frac{E_{0T}E_{0T}^*}{E_{0I}E_{0I}^*} = \frac{t^4 e^{-i\delta/2}e^{i\delta/2}}{(1 - r^2e^{-i\delta})(1 - r^2e^{+i\delta})}$$

$$= \frac{t^4}{1 + r^4 - 2r^2\cos\delta} = \frac{(1 - r^2)^2}{1 + r^4 - 2r^2\cos\delta}$$

where we have used the lossless mirror condition $t^2 = 1 - r^2$ and one of the Euler identities. Note that this relation is in agreement with Eq. (7-49), which gives the transmittance of a parallel plate. Using Eq. (8-16), the trigonometric identity $\cos\delta = 1 - 2\sin^2(\delta/2)$, and simplifying a bit allows the transmittance to be put into the form of the Airy function,

$$T = \frac{1}{1 + [4r^2/(1 - r^2)^2]\sin^2(\delta/2)} \tag{8-24}$$

Coefficient of Finesse

Fabry called the square-bracketed factor in Eq. (8-24), which is a function only of the reflection coefficient r of the mirrors, the *coefficient of finesse*, F:

$$F = \frac{4r^2}{(1 - r^2)^2} \tag{8-25}$$

Equation (8-24) can then be expressed more compactly as

$$T = \frac{1}{1 + F\sin^2(\delta/2)} \tag{8-26}$$

The coefficient of finesse is a sensitive function of the reflection coefficient r since, as r varies from 0 to 1, F varies from 0 to infinity. We show that F also represents a certain measure of *fringe contrast*, written as the ratio

$$\frac{(I_T)_{\max} - (I_T)_{\min}}{(I_T)_{\min}} = \frac{T_{\max} - T_{\min}}{T_{\min}} \tag{8-27}$$

From the Airy formula, Eq. (8-26), T takes on its maximum value $T_{\max} = 1$, when $\sin(\delta/2) = 0$, and its minimum value $T_{\min} = 1/(1 + F)$, when $\sin(\delta/2) = \pm 1$. Thus,

$$\frac{(I_T)_{\max} - (I_T)_{\min}}{(I_T)_{\min}} = \frac{1 - 1/(1 + F)}{1/(1 + F)} = F \tag{8-28}$$

Note that this measure of *fringe contrast*, the coefficient of finesse, differs from the related quantity, introduced in Chapter 7 as Eq. (7-17), called the *visibility*. The fringe profile may be plotted once a value of r is chosen. Such a plot, for several choices of r, is given in Figure 8-9. For each curve, we see that $T = T_{\max} = 1$ at $\delta = m(2\pi)$, and $T = T_{\min} = 1/(1 + F)$ at $\delta = (m + 1/2)2\pi$. Notice that $T_{\max} = 1$ regardless of r and that $T_{\min}$ is never zero but approaches this value as r approaches 1. For real mirrors with absorption losses, the maximum transmittance is somewhat less than unity. The transmittance peaks sharply at higher values of r as the phase difference approaches integral multiples of 2π, remaining near zero for most of the region between fringes. As r increases even more to an attainable value of 0.97, for example, F increases to 1078 and the fringe widths are less than a third of

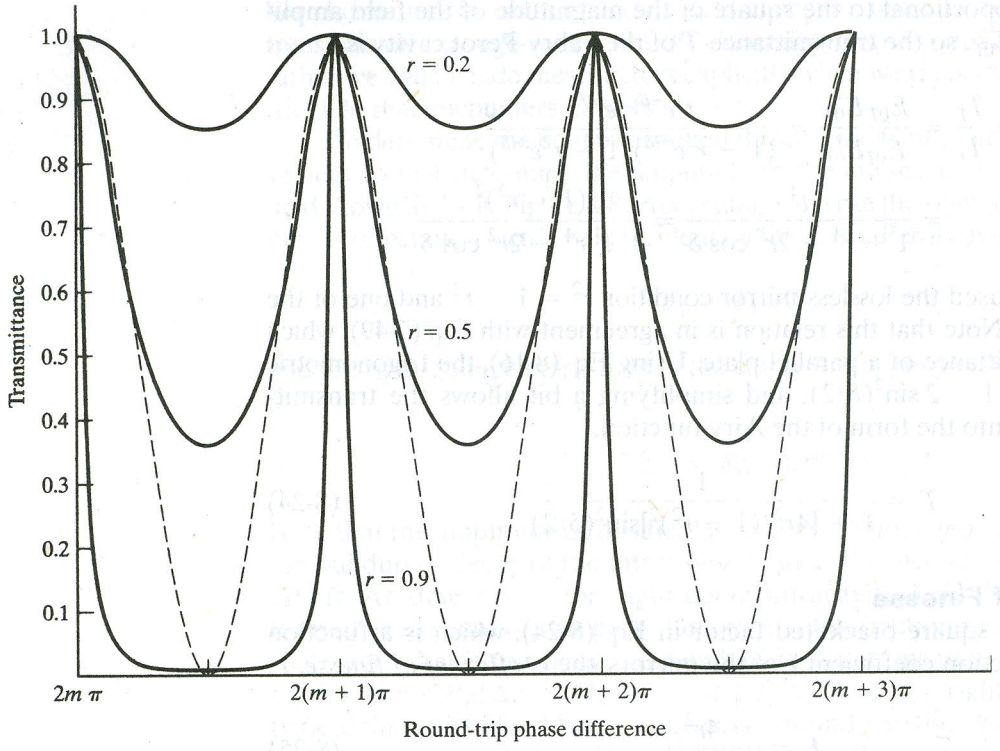

Figure 8-9 Fabry-Perot fringe profile. A plot of transmittance T versus round-trip phase difference δ for selected values of reflection coefficient r. Dashed lines represent comparable fringes from a Michelson interferometer.

their values at half-maximum for $r = 0.9$. The sharpness of these fringes is to be compared with the broader fringes from a Michelson interferometer, which have a simple $\cos^2(\delta/2)$ dependence on the phase (Eq. (8-2)). These are also shown in Figure 8-9 by the dashed lines, normalized to a maximum value of 1.

Finesse

The *coefficient of finesse* F is not to be confused with a second commonly used figure of merit $\mathcal{F}$, called simply the *finesse*:

$$\mathcal{F} = \frac{\pi\sqrt{F}}{2} = \frac{\pi r}{1 - r^2} \tag{8-29}$$

We now show that the finesse $\mathcal{F}$ is the ratio of the separation between transmittance peaks to the full-width at half-maximum (FWHM) of the peaks. Equations (8-26) and (8-29) can be combined to write the transmittance as

$$T = \frac{1}{1 + (4\mathcal{F}^2/\pi^2)\sin^2(\delta/2)} \tag{8-30}$$

The phase separation between adjacent transmittance peaks is sometimes called the *free spectral range* (FSR) of the cavity, δ_{fsr}. Thus,

$$\delta_{fsr} = \delta_{m+1} - \delta_m = (m + 1)2\pi - m2\pi = 2\pi$$

The half-width at half-maximum (HWHM) $\delta_{1/2}$ of the transmittance peaks (see Figure (8-10)) can be found from Eq. (8-30) by showing that when $T = 1/2$,

$$\sin^2(\delta/2) = \frac{\pi^2}{4\mathcal{F}^2} \tag{8-31}$$

where

$$\delta = 2m\pi + \delta_{1/2}$$

Trigonometric identities and a small angle approximation can be used to verify that, at the half-maxima,

$$\sin^2(\delta/2) = \sin^2(m\pi + \delta_{1/2}/2) = \sin^2\left(\frac{\delta_{1/2}}{2}\right) \approx \left(\frac{\delta_{1/2}}{2}\right)^2 \qquad (8\text{-}32)$$

Combining Equations (8-31) and (8-32), we find that

$$\delta_{1/2} = \pi/\mathcal{F} \qquad (8\text{-}33)$$

Cavities with more highly reflecting mirrors have higher values for the finesse and so narrower transmittance peaks than do cavities with less highly reflecting mirrors. As suggested, the finesse of a cavity is the ratio of the free spectral range of the cavity to the FWHM of the cavity transmittance peaks:

$$\frac{\delta_{fsr}}{\text{FWHM}} = \frac{2\pi}{2\delta_{1/2}} = \mathcal{F} \qquad (8\text{-}34)$$

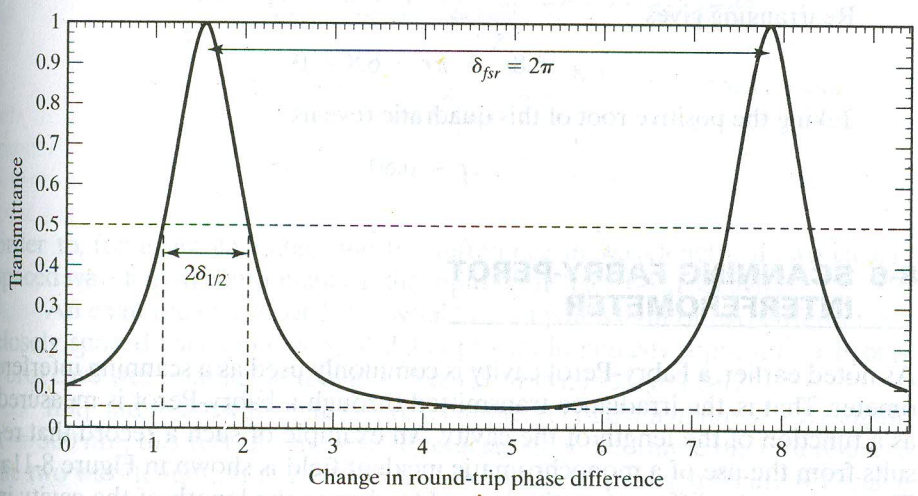

Figure 8-10 Transmittance T as a function of round-trip phase shift δ. The parameters used to produce this plot are discussed in Example 8-2.

The transmittance may be regarded as a function of the round-trip phase shift δ or any of the factors upon which δ depends, such as the mirror spacing (cavity length) d, the frequency ν (and so wavelength λ) of the input field, or the index of refraction n of the medium in the space between the mirrors. In different modes of operation, one of these quantities is typically varied while the others are held constant. Although the values of the free spectral range and the FWHM of the transmittance peaks depend, of course, on the chosen independent variable, the ratio of these quantities (i.e., the finesse) depends only on the reflectivities of the mirrors and so is a useful figure of merit for the Fabry-Perot cavity. We shall use the *term* free spectral range to refer to the separation between adjacent transmittance peaks regardless of the choice of independent variable but take care to *symbolically* differentiate between the free spectral ranges in the different modes of operation. For example, we shall give the free spectral range of a variable-length Fabry-Perot interferometer the symbol d_{fsr} and that of a variable-input-frequency Fabry-Perot interferometer the symbol ν_{fsr}.

Example 8-2

Estimate the coefficient of finesse F, the finesse $\mathcal{F}$, and the mirror reflectivity r for a Fabry-Perot cavity with the transmittance curve shown in Figure 8-10.

Solution

Using Eq. (8-27) and noting from Figure 8-10 that $T_{min} = 0.05$, the coefficient of finesse is found to be

$$F = \frac{T_{max} - T_{min}}{T_{min}} \approx \frac{1 - 0.05}{0.05} = 19$$

The finesse can be found either by extracting the FWHM from Figure 8-10 and using Eq. (8-34),

$$\mathcal{F} = \frac{\delta_{fsr}}{\text{FWHM}} \approx \frac{2\pi}{2.03 - 1.11} = 6.8$$

or by using Eq. (8-29),

$$\mathcal{F} = \frac{\pi\sqrt{F}}{2} \approx \frac{\pi\sqrt{19}}{2} = 6.8$$

The mirror reflection coefficient can be obtained from Eq. (8-29),

$$\mathcal{F} = \frac{\pi r}{(1 - r^2)} = 6.8$$

Rearranging gives

$$6.8r^2 + \pi r - 6.8 = 0$$

Taking the positive root of this quadratic reveals

$$r \approx 0.80$$

8-6 SCANNING FABRY-PEROT INTERFEROMETER

As noted earlier, a Fabry-Perot cavity is commonly used as a scanning interferometer. That is, the irradiance transmitted through a Fabry-Perot is measured as a function of the length of the cavity. An example of such a record that results from the use of a monochromatic incident field is shown in Figure 8-11a. There are many different methods used to change the length of the cavity in a controlled fashion. For example, if the Fabry-Perot interferometer consists of two mirrors separated by an air gap, the mirror separation can be controlled by means of a piezoelectric spacer, as shown in the Figure 8-11b. The transmittance is a maximum whenever

$$\delta = 2kd = 2\frac{2\pi}{\lambda}d = 2m\pi \qquad m = 0, \pm 1, \pm 2 \ldots$$

Rearrangement gives the condition for a maximum as

$$d_m = m\lambda/2 \tag{8-35}$$

Accordingly, the free spectral range in this mode of operation is

$$d_{fsr} = d_{m+1} - d_m = \lambda/2 \tag{8-36}$$

The cavity length change required to move from one transmittance peak to another is thus a measure of the wavelength of the source. In practice, however, this relation, by itself, is not used to experimentally determine the wavelength of the source because the length change cannot be measured with the desired accuracy. Instead, Eq. (8-36) can be used to calibrate the length change of the cavity in

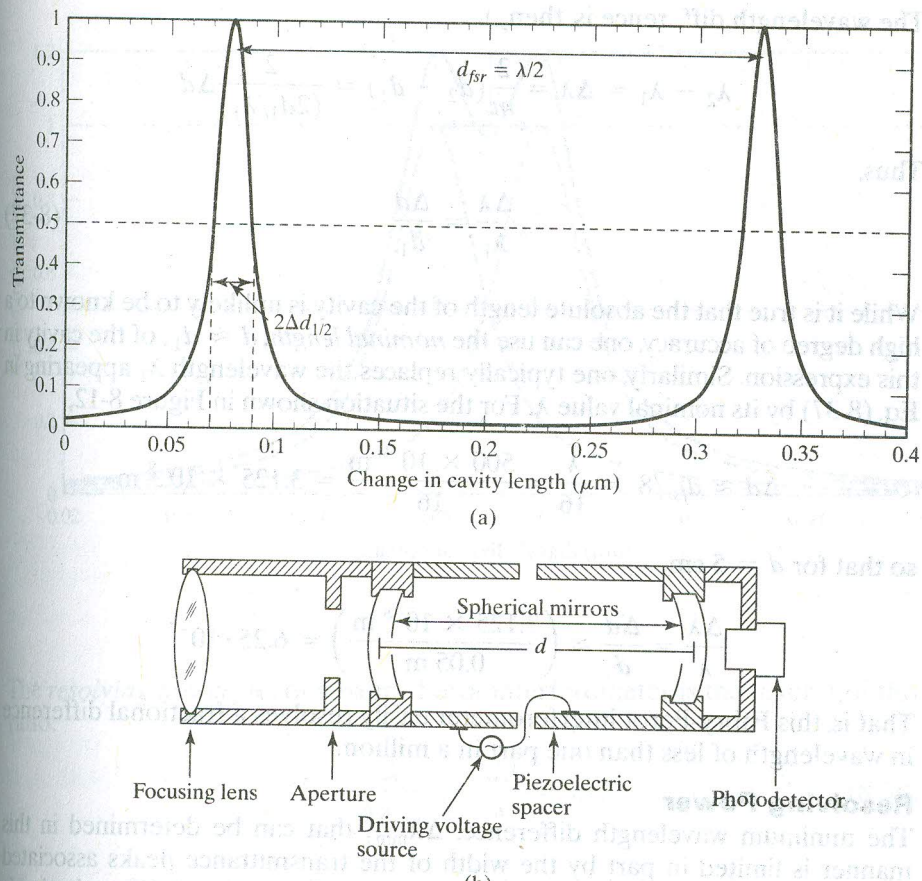

Figure 8-11 (a) Transmittance T as a function of the change in cavity length Δd, for a monochromatic input field. (b) Piezoelectric spacer used to control the mirror separation d.

order to, for example, determine the difference in wavelength of two closely spaced wavelength components in the input to the Fabry-Perot cavity.

An example of a record that would result when light of two different but closely spaced wavelengths λ_1 and λ_2 are simultaneously input into a Fabry-Perot cavity of nominal length $d = 5$ cm is shown in Figure 8-12.

If λ_1 and λ_2 are known to be, for example, very near a *nominal wavelength*, $\lambda = 500$ nm, this record can be used to accurately determine the difference in the two wavelengths. If it is known that the adjacent peaks in Figure 8-12 have the same mode number m, then the wavelengths must satisfy the relations

$$\lambda_1 = 2d_1/m$$
$$\lambda_2 = 2d_2/m$$

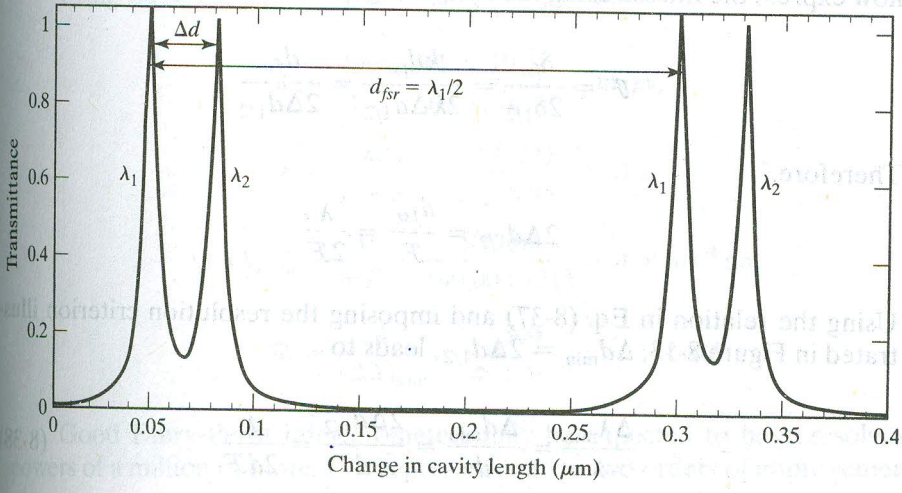

Figure 8-12 Fabry-Perot scan used to determine the difference in wavelength of two closely spaced wavelength components of the input field. The scan is for a nominal wavelength of 500 nm and a nominal mirror spacing of 5 cm.

The wavelength dif' .rence is, then,

$$\lambda_2 - \lambda_1 = \Delta\lambda = \frac{2}{m}(d_2 - d_1) = \frac{2}{(2d_1/\lambda_1)}\Delta d$$

Thus,

$$\frac{\Delta\lambda}{\lambda_1} = \frac{\Delta d}{d_1} \tag{8-37}$$

While it is true that the absolute length of the cavity is unlikely to be known to a high degree of accuracy, one can use the *nominal length*, $d \approx d_1$, of the cavity in this expression. Similarly, one typically replaces the wavelength λ_1 appearing in Eq. (8-37) by its nominal value λ. For the situation shown in Figure 8-12,

$$\Delta d \approx d_{fsr}/8 = \frac{\lambda}{16} = \frac{500 \times 10^{-9}\,\text{m}}{16} = 3.125 \times 10^{-8}\,\text{m}$$

so that for $d = 5$ cm,

$$\frac{\Delta\lambda}{\lambda} = \frac{\Delta d}{d} \approx \left(\frac{3.125 \times 10^{-8}\,\text{m}}{0.05\,\text{m}}\right) = 6.25 \cdot 10^{-7}$$

That is, this Fabry-Perot interferometer easily resolves a fractional difference in wavelength of less than one part in a million.

Resolving Power

The minimum wavelength difference, $\Delta\lambda_{\text{min}}$, that can be determined in this manner is limited in part by the width of the transmittance peaks associated with the two wavelength components. A commonly used resolution criterion is that the minimum *resolvable* difference, Δd_{min}, between the cavity lengths associated with the centers of the peaks of the transmittance functions of the two wavelength components is equal to the FWHM of these peaks. In this way, the crossover point of the two peaks will be not more than one-half of the maximum irradiance of either peak. This *resolution criterion*, $\Delta d \geq 2\,\Delta d_{1/2} \equiv \Delta d_{\text{min}}$, is illustrated in Figure 8-13.

We now show that the minimum resolvable wavelength difference, $\Delta\lambda_{\text{min}}$, can be compactly expressed in terms of the cavity finesse $\mathcal{F}$. As indicated by Eq. (8-29), the finesse of a Fabry-Perot cavity depends only on the reflection coefficient r of the cavity mirrors. As we mentioned, the finesse is a useful figure of merit because it is the ratio of the separation between adjacent transmittance peaks (that is, the cavity free spectral range) to the FWHM of a transmittance peak. Previously, as Eq. (8-34), we formed this ratio using the round-trip phase shift δ as the independent variable. Noting that $\delta = 2kd$, we now express the finesse using the cavity length d as the independent variable:

$$\mathcal{F} = \frac{\delta_{fsr}}{2\delta_{1/2}} = \frac{kd_{fsr}}{2k\Delta d_{1/2}} = \frac{d_{fsr}}{2\Delta d_{1/2}}$$

Therefore,

$$2\Delta d_{1/2} = \frac{d_{fsr}}{\mathcal{F}} = \frac{\lambda}{2\mathcal{F}}$$

Using the relation in Eq. (8-37) and imposing the resolution criterion illustrated in Figure 8-13, $\Delta d_{\text{min}} = 2\Delta d_{1/2}$, leads to

$$\frac{\Delta\lambda_{\text{min}}}{\lambda} = \frac{\Delta d_{\text{min}}}{d} = \frac{2\Delta d_{1/2}}{d} = \frac{\lambda}{2d\mathcal{F}} \tag{8-38}$$

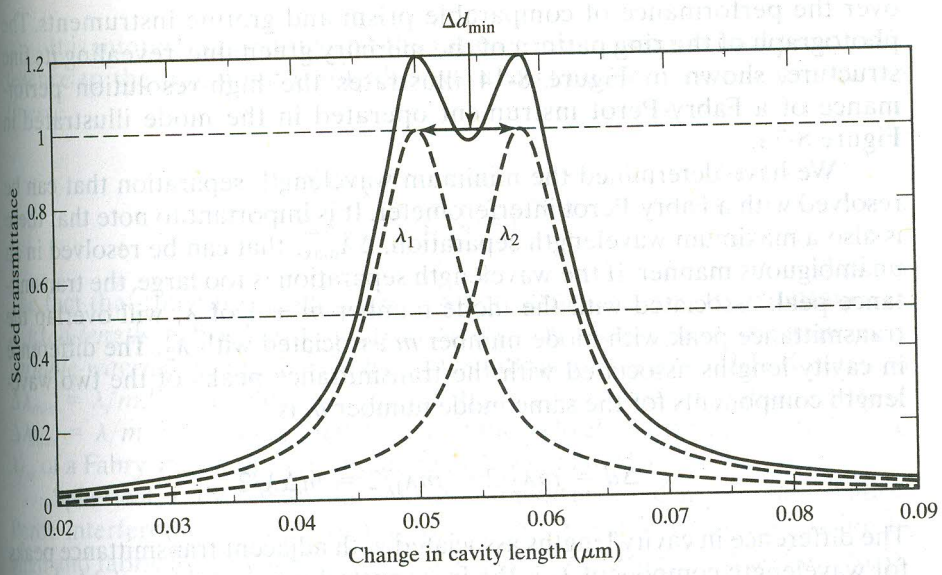

Figure 8-13 Scan of the (scaled) Fabry-Perot transmittance of two wavelength components of comparable strength. The dotted curves indicate the transmittance of the two wavelength components considered separately, and the solid curve is the scaled transmittance when both components are present in the input field. Note that these wavelength components are just barely resolved since the peaks are separated by a FWHM of either dotted curve.

The *resolving power*, $\mathcal{R}$, of a Fabry-Perot interferometer is the inverse of this ratio:

$$\mathcal{R} \equiv \frac{\lambda}{\Delta\lambda_{\min}} = \frac{2d\mathcal{F}}{\lambda} = m\mathcal{F} \tag{8-39}$$

Here, $m = 2d/\lambda$ is the mode number associated with the nominal wavelength λ and nominal cavity length d.

Large resolving powers are, of course, desirable. For the scanning Fabry-Perot interferometer, we see that large values occur when the mode number is large and for large values of the finesse, which occurs for reflection coefficients close to unity. Notice that to maximize the mode number m, Eq. (8-35) requires that the plate separation d be as large as possible.

Example 8-3

A Fabry-Perot interferometer has a 1-cm spacing between mirrors and a reflection coefficient of $r = 0.95$. For a wavelength around 500 nm, determine its mode number, its finesse, its minimum resolvable wavelength interval, and its resolving power.

Solution

Using Eqs. (8-35), (8-29), (8-38) and (8-39), we find

$$m = \frac{2d}{\lambda} = \frac{2(1 \times 10^{-2})}{500 \times 10^{-9}} = 40{,}000$$

$$\mathcal{F} = \frac{\pi r}{1 - r^2} = \frac{\pi(0.95)}{1 - 0.95^2} = 31$$

$$(\Delta\lambda)_{\min} = \frac{\lambda}{m\mathcal{F}} = \frac{500 \text{ nm}}{(40{,}000)(31)} = 4 \times 10^{-4} \text{ nm}$$

$$\mathcal{R} = \frac{\lambda}{(\Delta\lambda)_{\min}} = \frac{500}{4 \times 10^{-4}} = 1.2 \times 10^{6}$$

Good Fabry-Perot interferometers may be expected to have resolving powers of a million or more. This represents one to two orders of improvement

over the performance of comparable prism and grating instruments. The photograph of the ring pattern of the mercury green line, revealing its fine structure, shown in Figure 8-14 illustrates the high-resolution performance of a Fabry-Perot instrument operated in the mode illustrated in Figure 8-7a.

We have determined the minimum wavelength separation that can be resolved with a Fabry-Perot interferometer. It is important to note that there is also a maximum wavelength separation, $\Delta\lambda_{max}$, that can be resolved in an unambiguous manner. If the wavelength separation is too large, the transmittance peak associated with the mode number $m + 1$ of λ_1 will overlap the transmittance peak with mode number m associated with λ_2. The difference in cavity lengths associated with the transmittance peaks of the two wavelength components for the same mode number m is

$$\Delta d = m\lambda_2/2 - m\lambda_1/2 = m\Delta\lambda/2$$

The difference in cavity lengths associated with adjacent transmittance peaks for wavelength component λ_1 is the free spectral range of the variable-length Fabry-Perot interferometer,

$$d_{fsr} = (m + 1)\lambda_1/2 - m\lambda_1/2 = \lambda_1/2$$

The transmittance peak associated with the mode number $m + 1$ of λ_1 will overlap the transmittance peak with mode number m associated with λ_2 if $\Delta d = d_{fsr}$. That is, the overlap occurs if

$$m\Delta\lambda/2 = \lambda_1/2$$

Thus, the maximum wavelength separation that can be unambiguously resolved is

$$\Delta\lambda_{max} = \lambda_1/m \approx \lambda/m$$

Here, λ is the nominal wavelength of the incident light composed of the two closely spaced wavelength components λ_1 and λ_2. We note that wavelength separations larger than λ/m can be measured with a Fabry-Perot cavity provided that one has additional knowledge of the wavelength separation so that the difference in mode number associated with adjacent transmission peaks can be unambiguously determined.

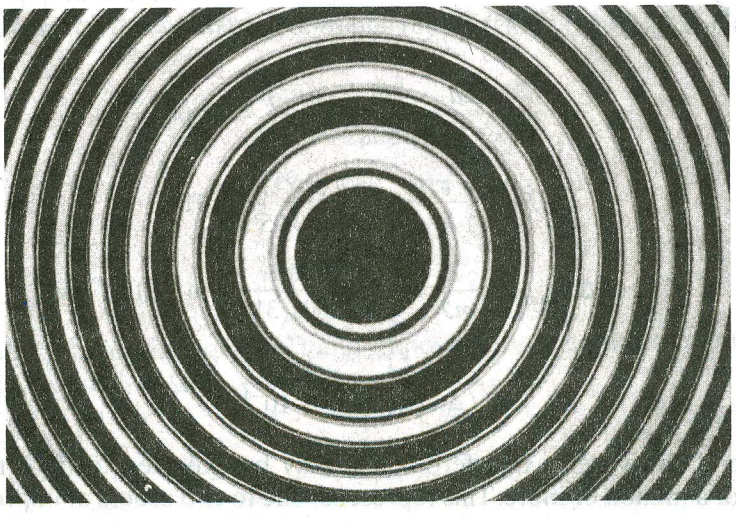

igure 8-14 Fabry-Perot rings obtained with ne mercury green line, revealing fine structure. (Reproduced by permission from "Atlas of Optical Phenomena", 1962, Michael Cagnet, Maurice Franco and Jean Claude Thrierr; Plate 0(top). Copyright© Springer-Verlag GmbH & Co KG. With Kind Permission of Springer Science and Business Media.)

It is interesting to note that the ratio of this maximum wavelength difference to the minimum resolvable wavelength difference is given by the finesse,

$$\frac{\Delta\lambda_{\max}}{\Delta\lambda_{\min}} = \frac{\lambda/m}{\lambda/(m\mathcal{F})} = \mathcal{F}$$

The fact that this ratio is the finesse is not surprising. The transmittance of a *fixed-length* Fabry-Perot interferometer considered as a function of a *variable-wavelength*-input field has transmittance peaks of FWHM equal to $\Delta\lambda_{\min} = \lambda/m\mathcal{F}$ and a peak separation (that is, a free spectral range) equal to $\Delta\lambda_{\max} = \lambda/m$. Thus, $\Delta\lambda_{\max}$ may be called the (wavelength) free spectral range λ_{fsr} of a Fabry-Perot interferometer. (See problem 8-23.)

Spherical, rather than flat, mirrors are often used in scanning Fabry-Perot interferometers. Spherical-mirror Fabry-Perot cavities are easier to align and fabricate and have greater light-gathering power than do flat-mirror cavities. However, spherical-mirror cavities also have a more complex transmittance spectrum than do the flat-mirror cavities just considered. Like cavities made from flat mirrors, spherical-mirror cavities have (so-called longitudinal) modes separated by the cavity free spectral range, but in addition they have (so-called transverse) modes associated with the relationship of the curvatures of the mirrors to the cavity length. The nature of the transverse modes of a cavity is discussed in more detail in Chapter 27. The more complicated mode structure associated with spherical-mirror Fabry-Perot cavities provides the possibility of additional markers that may be useful in the calibration of the Fabry-Perot interferometer.

8-7 VARIABLE-INPUT-FREQUENCY FABRY-PEROT INTERFEROMETERS

For the scanning Fabry-Perot cavity discussed in the previous section, the transmittance through the Fabry-Perot cavity is a function of the changing length of the cavity. A second variant of the Fabry-Perot interferometer uses a cavity of fixed length and a variable-frequency input field. In this mode of operation, the frequencies associated with the transmittance peaks provide frequency markers that can be used to monitor and calibrate the changing frequency of the input laser field. The free spectral range and FWHM of the transmittance T through a variable-input-frequency Fabry-Perot interferometer can be derived in a manner similar to that used in the discussion of the scanning Fabry-Perot interferometer of the last section. To do so, we should first relate the round-trip phase shift δ to the frequency of the input field ν. Making use of the fundamental relation $k = 2\pi/\lambda = 2\pi\nu/c$, the round-trip phase shift δ associated with an input field of frequency ν can be written as

$$\delta = 2kd = 4\pi(\nu/c)d$$

Thus, a record of the transmittance as a function of the variable input frequency will have maxima when the frequency of the input field has values that follow from the *resonance* condition,

$$\delta_m = 4\pi(\nu_m/c)d = 2m\pi \qquad m = 0, \pm1, \pm2\ldots$$

That is, the resonant frequencies of the Fabry-Perot cavity are

$$\nu_m = mc/2d \tag{8-40}$$

Note that we are assuming, here, that the index of refraction of the material in the space between the cavity mirrors is $n = 1$. In this mode of operation, the free spectral range of the interferometer is

$$\nu_{fsr} = \nu_{m+1} - \nu_m = c/2d \tag{8-41}$$

In fact, the term *free spectral range* is most commonly applied for this case, that is, when the transmittance is considered as a function of input frequency. The FWHM $2\Delta\nu_{1/2}$ of the transmittance curves can be found from the basic expression for $\mathcal{F}$ and the relation between round-trip phase shift δ and frequency ν. That is,

$$\mathcal{F} = \frac{\delta_{fsr}}{2\delta_{1/2}} = \frac{4\pi(\nu_{fsr}/c)d}{2[4\pi(\Delta\nu_{1/2}/c)d]} = \frac{\nu_{fsr}}{2\Delta\nu_{1/2}}$$

so that

$$2\Delta\nu_{1/2} = \frac{\nu_{fsr}}{\mathcal{F}}$$

Using Eq. (8-41) and the expression for the finesse $\mathcal{F}$ given in Eq. (8-29) gives

$$2\Delta\nu_{1/2} = \frac{c}{2d}\frac{1-r^2}{\pi r} \tag{8-42}$$

The transmittance through a Fabry-Perot interferometer as a function of the frequency of the input field is shown in Figure 8-15. A Fabry-Perot cavity used in this manner is often characterized by a *quality factor, Q*, defined as the ratio of a nominal resonant frequency to the FWHM of the transmittance peaks,

$$Q = \frac{\nu}{2\Delta\nu_{1/2}} = \mathcal{F}\frac{\nu}{\nu_{fsr}} \tag{8-43}$$

As noted, the transmittance of a Fabry-Perot interferometer, with an input laser field whose frequency is intentionally changed, can be used to calibrate the frequency change of the laser. The laser frequency could be changed, for example by changing the effective length of the laser cavity. Such a calibration procedure is useful, for example, in absorption spectroscopy.

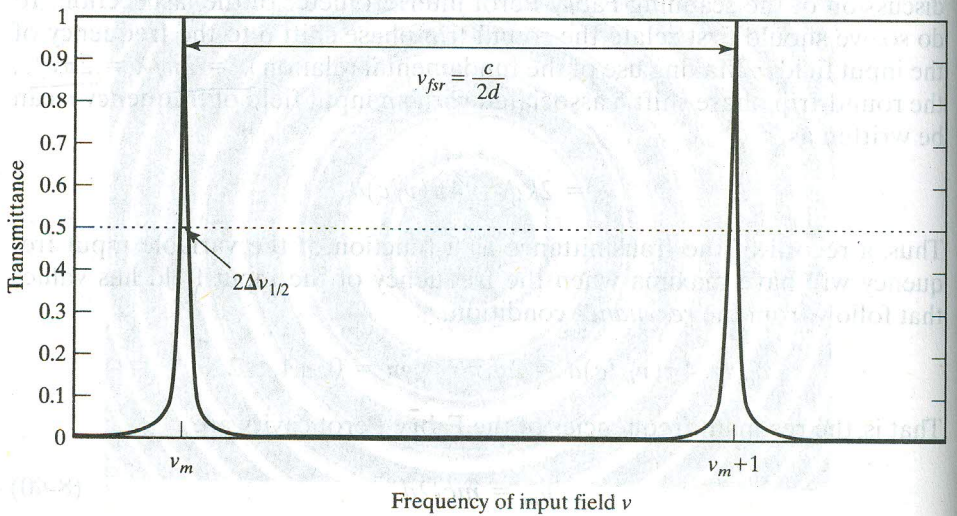

Figure 8-15 Transmittance T through a Fabry-Perot interferometer of fixed length d as a function of the variable frequency ν of the input field.

This application of a variable-input-frequency Fabry-Perot interferometer is explored in problem 8-22. Alternatively, as discussed at the end of the next section, the change in the transmittance through a fixed-length Fabry-Perot cavity induced by a change in the frequency of the laser input field can be used as a feedback signal to stabilize the frequency of the laser source.

In Example 8-4 we explore the relationships between various figures of merit for a variable-input-frequency Fabry-Perot interferometer.

Example 8-4

Consider the transmittance through a variable-input-frequency Fabry-Perot interferometer. Let the Fabry-Perot cavity have length $d = 5$ cm and finesse $\mathcal{F} = 30$. Take the nominal frequency of the laser to be $\nu = 5 \times 10^{14}$ Hz.

a. Find the free spectral range, ν_{fsr}, of this Fabry-Perot cavity.
b. Find the FWHM $2\Delta\nu_{1/2}$ of the transmittance peaks.
c. Find the quality factor Q of this Fabry-Perot cavity.
d. Estimate the smallest frequency change that could be easily monitored with this Fabry-Perot cavity.

Solution

a. Using Eq. (8-41), $\nu_{fsr} = \dfrac{c}{2d} = \dfrac{3 \times 10^8 \text{ m/s}}{2(0.05 \text{ m})} = 3 \text{ GHz}.$

b. Using the expression for the finesse, $\mathcal{F} = \dfrac{\nu_{fsr}}{2\Delta\nu_{1/2}}$, we find

$$2\Delta\nu_{1/2} = \nu_{fsr}/\mathcal{F} = (3 \text{ GHz})/30 = 100 \text{ MHz}.$$

c. Using Eq. (8-43), $Q = \dfrac{\nu}{2\Delta\nu_{1/2}} = \dfrac{5 \times 10^{14} \text{ Hz}}{10^8 \text{ Hz}} = 5 \times 10^6$

d. If the frequency is originally adjusted to give maximum transmittance, a frequency change of $\Delta\nu = \Delta\nu_{1/2} = 50$ MHz would cause the transmittance to fall by a factor of 2. Thus, it would be easy to monitor a frequency change of 50 MHz with this Fabry-Perot.

8-8 LASERS AND THE FABRY-PEROT CAVITY

Laser cavities typically consist of two highly reflecting spherical mirrors and so have the same basic structure as spherical-mirror Fabry-Perot cavities. The frequencies for which a fixed-length Fabry-Perot cavity has maximum transmittance are also the frequencies for which the light generated in a laser medium, within the same cavity, would experience low loss. In addition, as we show later, the rate at which light energy stored in an optical cavity decreases over time due to transmission through and absorption by the cavity mirrors is directly related to the FWHM, $2\Delta\nu_{1/2}$, of the transmittance peaks of the same cavity used as a Fabry-Perot interferometer. This cavity loss rate, often called the *cavity decay rate* and given the symbol Γ, must be compensated for by the gain medium in order to maintain steady-state laser operation. The formalism introduced in Section 8-5 can be used to determine the rate at which the light energy stored in an optical cavity decreases over time. In particular, Eq. (8-21) can be adapted and used to develop an expression for the cavity loss rate. Let the field incident on a Fabry-Perot cavity be removed at time t_0. Further take the field in the cavity to be resonant with the cavity so that $\delta = 2m\pi$. Then for times $t > t_0$, Eq. (8-21) simplifies to

$$E_{01}^{+}(t+\tau) = r^2 E_{01}^{+}(t) \tag{8-44}$$

If, during one round-trip time τ the change in the complex field amplitude E_{01}^{+} is small compared to the amplitude itself, a Taylor series approximation can be used,

$$E_{01}^{+}(t+\tau) \approx E_{01}^{+}(t) + \tau \frac{d}{dt} E_{01}^{+}(t)$$

Using this in Eq. (8-44) and rearranging terms gives

$$\frac{d}{dt} E_{01}^{+}(t) = -\frac{1}{\tau}(1-r^2) E_{01}^{+}(t)$$

One can verify by direct substitution that the solution to this differential equation is

$$E_{01}^{+}(t) = E_{01}^{+}(t_0) e^{-(1/\tau)(1-r^2)(t-t_0)}$$

The right-going irradiance I^{+} in the cavity is proportional to the square of the magnitude of the complex field amplitude of the right-going wave, so

$$I^{+}(t) = I^{+}(t_0) e^{-(2/\tau)(1-r^2)(t-t_0)} \equiv I^{+}(t_0) e^{-\Gamma(t-t_0)}$$

That is, the cavity irradiance decays at the rate

$$\Gamma = \frac{2}{\tau}(1-r^2) \tag{8-45}$$

This sensible result indicates that, for lossless mirrors, the fractional irradiance loss $\Gamma\tau$ during each round-trip time τ is approximately $2(1-r^2) = 2t^2$. The inverse of the cavity decay rate Γ is sometimes called the *photon lifetime*, τ_p, of the cavity. That is, the photon lifetime of a cavity is the time interval $(t - t_0)$ over which the energy stored in a cavity without gain or input decays to $1/e$ of its initial value. If the light in the cavity is sustained by an input as in a Fabry-Perot cavity, or by a pumped gain medium as in the case of a laser, τ_p is the approximate time that a given portion of the light field remains in the cavity. Note that the approximate number of round-trips, N_{rt}, that a portion of the light field makes before exiting the cavity is, then,

$$N_{rt} \approx \frac{\tau_p}{\tau} = \frac{1}{2(1-r^2)} \tag{8-46}$$

It is useful to note (see Eqs. (8-42) and (8-45)) that, for highly reflective mirrors (r close to 1), the cavity decay rate and the FWHM of the transmittance peaks $2\Delta\nu_{1/2}$ are simply related:

$$\Gamma = \frac{2}{\tau}(1-r^2) = 2\pi r\left(\frac{c}{2d}\frac{1-r^2}{\pi r}\right) = 2\pi r(2\Delta\nu_{1/2}) \cong 2\pi(2\Delta\nu_{1/2})$$

This leads us to a second definition of the cavity quality factor Q as the ratio of the operating resonant cavity frequency $\omega = 2\pi\nu$ to the cavity decay rate:

$$Q \approx \frac{2\pi\nu}{\Gamma} = \frac{\omega}{\Gamma}$$

In addition to the formal similarity between Fabry-Perot and laser cavities, Fabry-Perot interferometers can serve a variety of roles as diagnostic or control elements in optical systems. For example, an external scanning Fabry-Perot interferometer provides a means of investigating the mode structure of the output of a multimode laser. Two common uses of the Fabry-Perot as a control element are as a means of limiting a laser to single-mode operation and as a component in a laser frequency stabilization system. These are discussed next.

Mode Suppression with an Etalon

As noted, many laser systems permit so-called multimode operation. That is, the steady-state output of the laser includes electric fields with frequencies corresponding to many different cavity resonances. In some applications, it is preferable for the laser to have an output at only a single cavity resonant frequency. Such a single-mode laser has a longer coherence length than a multimode laser. A Fabry-Perot etalon of length d can be inserted into a laser cavity of length $l > d$ in order to suppress all but a single laser mode.

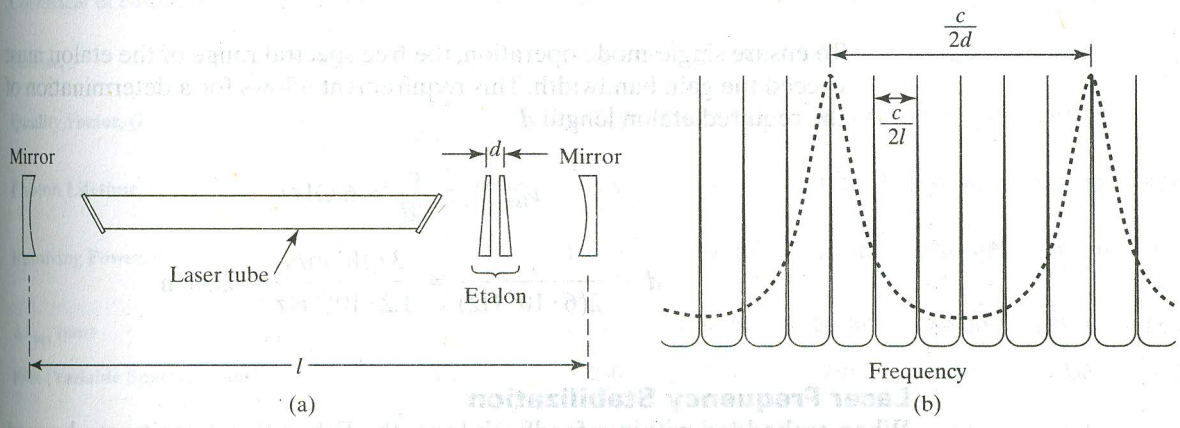

Figure 8-16 (a) Laser with intracavity etalon for single-mode operation. (b) Transmittance for laser cavity of length l (solid curve) and etalon of length d (dashed curve).

For a laser system like that shown in Figure 8-16a, a cavity mode of a given frequency will be present in the laser output only if it is amplified by the laser gain medium and satisfies also the low loss condition imposed by both the laser cavity and the etalon. The etalon, being much shorter than the laser cavity, has a free spectral range, $\nu_{fsr} = c/2d$, that is much larger than that of the laser cavity, $c/2l$. The length of the etalon can be chosen so that only a single etalon mode overlaps an existing cavity mode within the frequency range (the gain bandwidth) of laser operation. In addition, if the width of the etalon mode is less than the free spectral range of the cavity, only one cavity mode will be present in the laser output. Mode spacings in a typical laser system using an etalon for mode suppression are shown in Figure 8-16b. Tuning of the position of the etalon mode within the gain bandwidth can be accomplished by changing the effective etalon spacing d, for example, by piezoelectric control of the etalon spacing or by tilting the etalon. The use of an etalon to limit a laser to single mode operation is explored in Example 8-5.

Example 8-5

A certain argon-ion laser can support steady-state lasing over a range of frequencies of 6 GHz. That is, the gain bandwidth of the argon-ion laser is about 6 GHz. If the length of the laser cavity is $l = 1$ m, estimate the number of longitudinal cavity modes that might be present in the laser output. Also find the minimum length d of an etalon that could be used to limit this laser to single-mode operation.

Solution

The longitudinal cavity modes are separated by the free spectral range of the laser cavity,

$$\nu_{fsr}^{\text{laser}} = \frac{c}{2l} = \frac{3 \cdot 10^8 \text{ m/s}}{2(1 \text{ m})} = 0.15 \text{ GHz}$$

Therefore, the number of lasing modes would be given by

$$\#\text{ of lasing modes} \approx \frac{6 \text{ GHz}}{0.15 \text{ GHz}} = 40$$

To ensure single-mode operation, the free spectral range of the etalon must exceed the gain bandwidth. This requirement allows for a determination of the required etalon length d:

$$\nu_{fsr}^{\text{etalon}} = \frac{c}{2d} > 6 \text{ GHz}$$

$$d < \frac{c}{2(6 \cdot 10^9 \text{ Hz})} = \frac{3 \cdot 10^8 \text{ m/s}}{1.2 \cdot 10^{10} \text{ Hz}} = 2.5 \text{ cm}$$

Laser Frequency Stabilization

When embedded within a feedback loop, the Fabry-Perot cavity can be used to provide state-of-the-art frequency or length stabilization. For example, light output from a single-mode laser can be fed into a stabilized Fabry-Perot cavity adjusted to allow maximum transmission of this frequency of the laser light. When the laser frequency strays from the resonant frequency of the Fabry-Perot interferometer, the resultant dip in the transmittance of the Fabry-Perot can be used to initiate a feedback signal used to return the laser frequency to the resonant frequency of the Fabry-Perot cavity. Of course, such a system does not really stabilize the absolute frequency of the laser output but rather locks it to the resonant frequency of the Fabry-Perot. If the Fabry-Perot is in turn locked to a very stable frequency source of known frequency, absolute stabilization of the laser frequency is achieved.

8-9 FABRY-PEROT FIGURES OF MERIT

As we have seen, the Fabry-Perot interferometer is a flexible device that has many modes of operation. In Table 8-1 we list relations involving some figures of merit for Fabry-Perot cavities. In Table 8-2, representative values of these figures of merit, as well as some other quantities, are listed for different mirror reflection coefficients. Note that in Table 8-2 there are two rows each for the FSR and FWHM: The values in one set are pertinent when the transmittance varies as a result of changing the mirror spacing d, and the values in the other set apply when the transmittance varies as a result of changing the input frequency ν.

TABLE 8-1 FABRY-PEROT FIGURES OF MERIT.
Here r is the end mirror reflection coefficient, T is the Fabry-Perot transmittance, R is the resolving power of the Fabry-Perot with an input field of nominal wavelength λ whose mirror spacing d is varied, $2\Delta\nu_{1/2}$ is the FWHM of a transmittance peak when the frequency of the input is varied around frequency ν, Γ is the decay rate of the light within the Fabry-Perot cavity, τ_p is the photon lifetime of the cavity, and FSR stands for free spectral range.

Coefficient of Finesse	$F = \dfrac{4r^2}{(1-r^2)^2}$	$T = \dfrac{1}{1 + F\sin^2(\delta/2)}$	$F = \dfrac{T_{\max} - T_{\min}}{T_{\min}}$
Finesse	$\mathcal{F} = \dfrac{\pi\sqrt{F}}{2} = \dfrac{\pi r}{1-r^2}$	$\mathcal{F} = \dfrac{\text{FSR}}{\text{FWHM}}$	$\mathcal{R} \equiv \dfrac{\lambda}{\Delta\lambda_{\min}} = \dfrac{2d\mathcal{F}}{\lambda}$
Quality Factor	$Q = \dfrac{\nu}{\nu_{fsr}}\mathcal{F}$	$Q = \dfrac{\nu}{2\Delta\nu_{1/2}}$	$Q \approx \dfrac{\omega}{\Gamma} = \omega\tau_p$

TABLE 8-2 Fabry-Perot parameters for a cavity with a nominal spacing of $d = 5$ cm, a nominal input wavelength of $\lambda = 500$ nm, and a nominal frequency of $\nu = 6 \cdot 10^{14}$ Hz. Photon lifetime and FWHM are quantities that are not applicable (NA) if the reflection coefficient is too low.

Mirror Reflection Coefficient	r	0.2	0.5	0.8	0.9	0.97	0.99
Coefficient of Finesse, F	$\dfrac{4r^2}{(1-r^2)^2}$	0.174	1.78	19.8	89.8	1080	9900
Finesse, $\mathcal{F}$	$\dfrac{\pi r}{1-r^2}$	0.655	2.09	6.98	14.9	51.6	156
Quality Factor, Q	$\dfrac{\nu}{(c/2d)}\mathcal{F}$	$1.31 \cdot 10^5$	$4.19 \cdot 10^5$	$1.40 \cdot 10^6$	$2.98 \cdot 10^6$	$1.03 \cdot 10^7$	$3.13 \cdot 10^7$
Photon Lifetime, τ_p (s)	$\dfrac{d}{c(1-r^2)}$	NA	NA	$4.63 \cdot 10^{-10}$	$8.77 \cdot 10^{-10}$	$2.82 \cdot 10^{-9}$	$8.38 \cdot 10^{-9}$
Resolving Power, $\mathcal{R}$	$\dfrac{2d\mathcal{F}}{\lambda}$	$1.31 \cdot 10^5$	$4.19 \cdot 10^5$	$1.40 \cdot 10^6$	$2.98 \cdot 10^6$	$1.03 \cdot 10^7$	$3.13 \cdot 10^7$
$\Delta\lambda_{\min}$ (nm)	$\dfrac{\lambda^2}{2d\mathcal{F}}$	$3.82 \cdot 10^{-3}$	$1.19 \cdot 10^{-3}$	$3.58 \cdot 10^{-4}$	$1.68 \cdot 10^{-4}$	$4.85 \cdot 10^{-5}$	$1.60 \cdot 10^{-5}$
FSR (Variable Spacing) (nm)	$\lambda/2$	250	250	250	250	250	250
FWHM (Variable Spacing) (nm)	$\dfrac{\lambda}{2\mathcal{F}}$	NA	NA	35.8	16.8	4.85	1.6
FSR (Variable Frequency) (GHz)	$\dfrac{c}{2d}$	3	3	3	3	3	3
FWHM (Variable Frequency) (GHz)	$\dfrac{c}{2d\mathcal{F}}$	NA	NA	0.43	0.202	0.0582	0.0192

8-10 GRAVITATIONAL WAVE DETECTORS

We conclude this chapter with a description of interferometers used for gravitational wave detection. At the time of this writing, members of the Laser Interferometer Gravitational Observatory (LIGO) project are building, at two different sites within the United States, interferometers designed to detect and study gravitational waves. Similar interferometers are being developed by scientists and engineers in Europe and Japan. Gravitational waves result from the acceleration of mass in a manner that is analogous to the generation of electromagnetic waves by the acceleration of charge. Gravitational waves exert time-varying forces on matter as they pass by. Because the gravitational force is so weak, gravitational waves coming from even the most dramatic astronomical events like the collision of black holes or the explosion of supernovae lead to extraordinarily small effects on earth. To date, gravitational waves have not been directly detected, but the interferometers currently being constructed are predicted to be sensitive enough to detect the gravitational waves